Dynamical spin correlation function in $CsCo_pMg_{1-p}Cl_3$

1992 J. Phys.: Condens. Matter 4 2641

(http://iopscience.iop.org/0953-8984/4/10/026)

J. Phys.: Condens. Matter 4 (1992) 2641–2650. Printed in the UK

Dynamical spin correlation function in $CsCo_pMg_{1-p}Cl_3$

K Murao, F Matsubara and S Inawashiro
Department of Applied Physics, Tohoku University, Sendai 980, Japan

Received 9 September 1991

Abstract. The dynamical spin correlation function $S^{xx}(Q, \omega)$ of dilute antiferromagnet $CsCo_pMg_{1-p}Cl_3$ is analysed using a one-dimensional Ising-like model of $S = 1/2$ with the nearest-neighbour interaction J and the next-nearest-neighbour interaction J'. Our results reproduce well the experimental results from Nagler *et al* (1984). We estimate $J'/J \sim 0.1$, which is compatible with a previous estimation. Two peaks found at $\omega \sim J$ and $\omega \sim 2J$ correspond to single soliton excitations and soliton-pair excitations, respectively. The interaction J' over a single Mg^{2+} ion broadens the peak at $\omega \sim J$. As the temperature is increased, another peak appears at $\omega \sim 0$.

1. Introduction

The dynamical properties of quasi-one-dimensional Ising-like antiferromagnet $CsCoCl_3$ have been studied extensively. Inelastic neutron scattering has been a major means of measuring the dynamical spin correlation function. The Villain mode peak (Villain 1975) was observed in $S^{xx}(Q, \omega)$ at $\omega \sim 0$ by inelastic neutron scattering in $CsCoCl_3$ for the first time by Hirakawa and Yoshizawa (1979), Yoshizawa *et al* (1981), and also in $CsCoBr_3$ by Nagler *et al* (1982, 1983b). Contrary to Villain's prediction, the experimental results did not show sharp shoulders. Recent simulations showed that this discrepancy could be removed by taking into account collisions among propagating domain walls (solitons) (Matsubara and Inawashiro 1990).

Another characteristic peak of $S^{xx}(Q, \omega)$ at $\omega \sim 2J$ was found in the neutron scattering experiments on $CsCoCl_3$ (Hirakawa and Yoshizawa 1979, Yoshizawa *et al* 1981) and on $CsCoBr_3$ (Nagler *et al* 1983a). Ishimura and Shiba (1980) explained this peak on the basis of a picture of soliton-pair excitations. However, their results were not in good agreement with the experimental observations of the Q-dependence of the peak position and the line shape. Shiba (1980) also analysed Raman scattering data (Breitling *et al* 1977a, b, c, Lehmann *et al* 1981) taking into account weak interchain interactions. He could explain the experimental data qualitatively, but there remained some discrepancies in the quantitative point of view. Matsubara and Inawashiro (1989) pointed out that a next-nearest-neighbour interaction along the chain contributes markedly on $S^{xx}(Q, \omega)$. Having taken into account the interaction, they could explain the results of neutron scattering experiments (Matsubara and Inawashiro 1991) and magnetic Raman scattering experiments (Matsubara *et al* 1991).

As for the dilute magnet $CsCo_pMg_{1-p}Cl_3$, one-dimensional Co^{2+} chains are randomly cut in segments by Mg^{2+} ions. Magnetic excitations of this compound were studied by

0953-8984/92/102641 + 10 $04.50

Table 1. The values of parameters estimated by various workers, where J, ε and J' are defined in the text and J_1 is the interchain interaction in the ab plane.

	J (K)	ε	J'/J	J_1/J
Lehmann *et al* (1981)	70.2	0.11 ~ 0.14	—	0.0125
Nagler *et al* (1984)	74.4	0.120	—	0.0500
Matsubara and Inawashiro (1991)	62.9	0.150	0.100	—
Matsubara *et al* (1991)	63.6	0.145	0.095	0.0115
Present work	65.9	0.145	0.095	—

Nagler *et al* (1984), and two peaks were observed in $S^{xx}(Q, \omega)$. They also analysed the experimental data using the diagonalization technique. Based on the results of finite chains with up to eight spins, they identified the higher energy side peak ($\omega \sim 2J$ peak) as soliton-pair excitations and the lower energy side peak ($\omega \sim J$ peak) as a flip of the end spins of the chains. However, their results did not explain satisfactorily the Q-dependence of the $\omega \sim 2J$ peak and the relative intensities of the two peaks. Moreover, their identification of the $\omega \sim J$ peak is unacceptable from the point of view of a propagating domain wall (Villain 1975, Nagler *et al* 1983a,b).

In the present paper, the magnetic excitations in an Ising-like antiferromagnet with $S = 1/2$ on finite chains are discussed in detail, and then neutron scattering data of $CsCo_{0.83}Mg_{0.17}Cl_3$ are analysed. In section 2, the excitations in an isolated chain are discussed. In section 3, formulation and calculation for the dilute system are presented with and without interchain interaction. Comparison with the experimental data is made in section 4. Section 5 is devoted to the summary.

2. Dynamical spin correlation in an isolated chain

In $CsCo_pMg_{1-p}Cl_3$, finite chains of Co^{2+} ions along the c-axis are separated by non-magnetic Mg^{2+} ions. Magnetic quantities are described by a weighted sum of the corresponding quantities of these chains. Hence, we first study the dynamical spin correlation in the finite chains. There are two kinds of interactions among those finite chains; one is the next-nearest-neighbour interaction along the c-axis over an isolated single Mg^{2+} ion, the other is the interchain interaction in the ab-plane. The former will be discussed in the next section. The magnitude of the latter was estimated to be 1% of the nearest-neighbour interaction in $CsCoCl_3$ as shown in table 1 (Shiba 1980, Lehmann *et al* 1981, Matsubara and Inawashiro 1991, Matsubara *et al* 1991). The effect of the interaction will be more weakened in $CsCo_pMg_{1-p}Cl_3$ because of the randomness, so we will ignore it throughout this paper.

2.1. Hamiltonian and dynamical spin correlation function $S_n^{xx}(Q, \omega)$

Let our model Hamiltonian of n-spin chain be

$$\mathcal{H} = \mathcal{H}_1 + \mathcal{H}_2 \tag{2.1a}$$

$$\mathcal{H}_1 = 2J \sum_{i=1}^{n-1} \{S_i^z S_{i+1}^z + \varepsilon(S_i^x S_{i+1}^x + S_i^y S_{i+1}^y)\} \tag{2.1b}$$

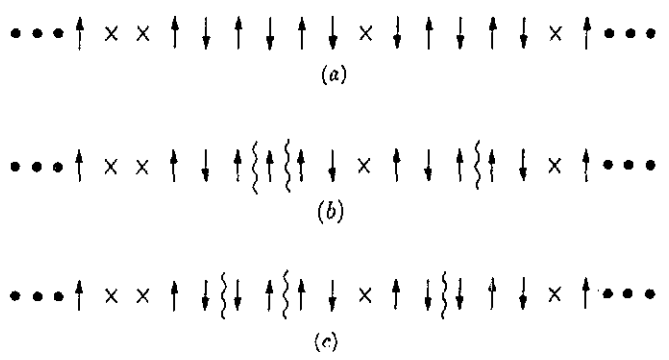

Figure 1. Low lying Ising states: (*a*) ground state, (*b*) and (*c*) excited states with up to two domain walls for each separated cluster.

$$\mathcal{H}_2 = -2J' \sum_{i=1}^{n-2} \{S_i^z S_{i+2}^z + \varepsilon(S_i^x S_{i+2}^x + S_i^y S_{i+2}^y)\} \tag{2.1c}$$

where J is the nearest-neighbour interaction, and J' is the next-nearest-neighbour interaction. Here, $\varepsilon \sim 0.1$, $J'/J \sim 0.1$ and the boundary condition is free.

Since the system is Ising-like ($\varepsilon \ll 1$), the Hamiltonian is diagonalized in a subspace consisting of low-lying Ising states. The ground state is described approximately by a Néel state (figure 1(*a*)). Reversing a right or left block of spins in a finite chain generates a domain wall between the two blocks with the energy loss of J ignoring the next-nearest-neighbour interaction J', as shown in figure 1(*b*). As we will see later, this mode appears as the $\omega \sim J$ peak in the $S^{xx}(Q, \omega)$. Similarly, reversing a middle block of spins generates a pair of domain walls (the left side cluster in figure 1(*b*)) and gives the $\omega \sim 2J$ peak in $S^{xx}(Q, \omega)$. Hence, for $T = 0$ K, the Ising states are chosen to have up to two domain walls. As for $T \neq 0$ K, the system is thermally excited, allowing transitions between excited states. So the Ising states are chosen to have up to four domain walls. Note that another mode arises at $\omega \sim 0$ for $T \neq 0$ K, which is illustrated as the transition between states described in figures 1(*b*) and (*c*).

The dynamical spin–correlation function is given by the space-time Fourier transformation of the spin–correlation function and is expressed by

$$S_n^{xx}(Q, \omega) = \frac{1}{Z} \sum_i \sum_f e^{-\beta E_i} |\langle \psi_f | S_{Qn}^x | \psi_i \rangle|^2 \delta(\omega - E_f + E_i). \tag{2.2a}$$

Here β denotes $1/k_B T$, E_i and E_f are the eigenvalues of the eigenstates ψ_i and ψ_f, respectively, and Z is the partition function given by

$$Z = \sum_i e^{-\beta E_i}. \tag{2.2b}$$

The operator S_{Qn}^x is the Fourier transformation of S_j^x

$$S_{Qn}^x = \sum_{j=1}^{n} S_j^x e^{iQR_j}. \tag{2.2c}$$

In order to investigate the contribution of the transition from the ground state and that of other transitions, we rewrite (2.2*a*) as follows.

$$S_n^{xx}(Q, \omega) = S_{nG}^{xx}(Q, \omega) + S_{nE}^{xx}(Q, \omega) \tag{2.3a}$$

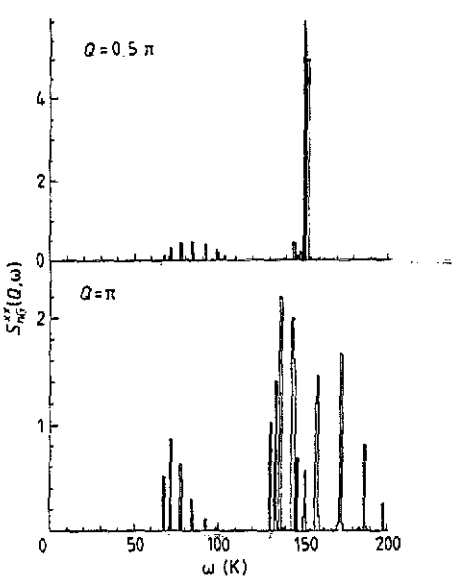

Figure 2. $S^{xx}_{nG}(Q, \omega)$ at $Q = 0.5\pi$ and π for $n = 15$ in the histogram with $\Delta\omega = 1$ K. The values of the parameters are given in table 1.

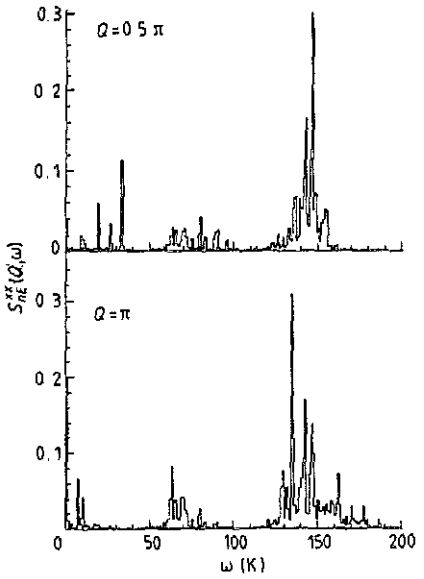

Figure 3. $S^{xx}_{nE}(Q, \omega)$ at $Q = 0.5\pi$ and π for $n = 11$ in the histogram with $\Delta\omega = 1$ K. The values of the parameters are given in table 1.

where

$$S^{xx}_{nG}(Q, \omega) = \frac{e^{-\beta E_g}}{Z} \sum_f |\langle \psi_f | S^x_{Qn} | \psi_g \rangle|^2 \delta(\omega - E_f + E_g) \tag{2.3b}$$

$$S^{xx}_{nE}(Q, \omega) = \frac{1}{Z} \sum_f \sum_{i \neq g} e^{-\beta E_i} |\langle \psi_f | S^x_{Qn} | \psi_i \rangle|^2 \delta(\omega - E_f + E_i) \tag{2.3c}$$

where, $|\psi_g\rangle$ is the ground state, and E_g is the ground state energy. $S^{xx}_{nG}(Q, \omega)$ describes the contribution of the transition from the ground state to excited states (GS → EX), and $S^{xx}_{nE}(Q, \omega)$ the transition between different excited states (EX → EX). For $T = 0$ K, the dynamical spin correlation is described by only $S^{xx}_{nG}(Q, \omega)$. However, when the temperature is increased, the relative intensity of $S^{xx}_{nE}(Q, \omega)$ increases while that of $S^{xx}_{nG}(Q, \omega)$ decreases because the factor $\exp(-\beta E_g)/Z$ decreases. Note that when the temperature is low and the energy of the first excited state is sufficiently high, we can still ignore $S^{xx}_{nE}(Q, \omega)$. This occurs, for instance, in such a case as $T = 4.7$ K, $E_1 - E_g = 60$ K where E_1 is the first excited state energy.

In the following, the results are shown separately for $S^{xx}_{nG}(Q, \omega)$ and $S^{xx}_{nE}(Q, \omega)$. The values of the parameters are chosen to be $J = 65.9$ K, $\varepsilon = 0.145$, $J'/J = 0.095$, keeping in mind the comparison with the experimental results.

2.2. $S^{xx}_{nG}(Q, \omega)$

Typical results of $S^{xx}_{nG}(Q, \omega)$ for $Q = 0.5\pi$ and π are shown in figure 2. These results were calculated by restricting the Ising states to two domain walls. The approximation was justified by the fact that the $S^{xx}_{nG}(Q, \omega)$ did not change substantially by extending the subspace of Ising states up to four domain walls. The peak at around 150 K is the

$\omega \sim 2J$ peak and the peak at around 75 K is the $\omega \sim J$ peak. The intensity of the $\omega \sim 2J$ peak is much stronger than that of the $\omega \sim J$ peak. This is due to the fact that the number of the soliton-pair states is ${}_{n-1}C_2 \sim n^2/2$ and the number of the single soliton states is ${}_{n-1}C_1 \sim n$, where n is the number of spins.

The $\omega \sim 2J$ peak is broad at $Q = \pi$ and sharp at $Q = 0.5\pi$. It exhibits a tail on the high energy side at $Q = \pi$. These results are similar to those obtained by Matsubara and Inawashiro (1991) in the chains with the periodic boundary condition.

The $\omega \sim J$ peak is broad and spreads over the range from 60 K to 100 K. This reveals that the $\omega \sim J$ mode is a delocalized (or propagating) mode where a single domain wall exists widely inside the chain, contrary to Nagler's conjecture. At $Q = \pi$, this peak is high on low energy side. At $Q = 0.5\pi$, the peak is lower and more flat.

2.3. $S^{xx}_{nE}(Q, \omega)$

The results of $S^{xx}_{nE}(Q, \omega)$ for $Q = 0.5\pi$ and π are shown in figure 3. The main difference from figure 2 is the occurrence of the $\omega \sim 0$ peak. This peak originates from the transition, represented by figures 1(b) and (c), which preserves the number of solitons, hence its Q-dependence shows the same character as the Villain mode, i.e. the broad peak with a shoulder at $Q = 0.5\pi$ and a sharp and intensive peak at $Q = \pi$.

Shapes of other peaks are similar to those of $S^{xx}_{nG}(Q, \omega)$, but they are smooth due to the broad dispersion of energy in the initial states.

3. Dynamical spin correlation in dilute systems

Now, we consider the dilute system, in which a dynamical spin correlation function is obtained by accumulating contributions from finite chains of various lengths. However, there are couplings between chains over a single Mg^{2+} ion, because there also exists superexchange interactions through Cl^- ions between next-nearest-neighbour Co^{2+}

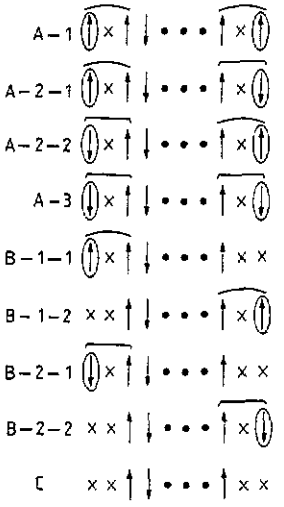

Figure 4. Types of molecular fields at the ends of chains. The probabilities of these occurring are given in table 2.

Table 2. Probabilities for types of molecular fields shown in figure 4. Concentration of Co^{2+} ions is given by p.

Type of molecular field	A–1	A–2–1	A–2–2	A–3	B–1–1	B–1–2	B–2–1	B–2–2	c
Thermal probability	1	$e^{-\beta J'}$	$e^{-\beta J'}$	$e^{-2\beta J'}$	1	1	$e^{-\beta J'}$	$e^{-\beta J'}$	1
Geometrical probability	p^2	p^2	p^2	p^2	$2p(1-p)$	$2p(1-p)$	$2p(1-p)$	$2p(1-p)$	$(1-p)^2$

ions, as assumed in the model Hamiltonian (2.1). For simplicity, we take into account the interactions by molecular fields and add the following term to the Hamiltonian

$$\mathcal{H}_{MF} = -2J'(S^z_1\langle S^z_{-1}\rangle + S^z_N\langle S^z_{N+2}\rangle) \tag{3.1}$$

Here, the molecular fields represented by $\langle S^z_{-1}\rangle$ and $\langle S^z_{N+2}\rangle$ are listed in figure 4 and table 2. In the figure, series A, B and C stand for configuration of non-magnetic ion and are found by the geometrical probability in the dilute system, where the concentration of Co^{2+} ions is given by p. Each series is divided into cases depending on whether the molecular fields and the spins at the ends of a chain are cooperative or non-cooperative. Here, these ratios are denoted as thermal probability.

We investigate the effect of the molecular fields on the dynamical spin correlation function. Figure 5 is the results of $S^{xx}_{nO}(Q, \omega)$ at $Q = \pi$. The $\omega \sim J$ peak strongly depends on the molecular fields. For example, the line shapes of the $\omega \sim J$ peak in A–1 and A–3 are almost the same but their positions are different, and the line shape in A–2–1 is different from the others. This is due to the fact that the $\omega \sim J$ peak comes from the flip of the end spin which is subject to the next-nearest-neighbour interaction over a single Mg^{2+} ion. On the other hand, since the $\omega \sim 2J$ peak comes from the flip of spins in the middle of the chain, it is affected little by the molecular fields as seen in figure 5. Figure 6 shows the results of $S^{xx}_{nE}(Q, \omega)$ at $Q = \pi$. The results for $\omega \sim J$ and $2J$ are similar to those in figure 5. The $\omega \sim 0$ peak is not strongly affected by the molecular fields. This is also due to the fact that this peak comes from the spin flip in the middle of the chain.

Hence, we calculate the dynamical spin correlation function averaged over the molecular fields and denote it as $\bar{S}^{xx}_n(Q, \omega)$. The total $S^{xx}(Q, \omega)$ is expressed in terms of the power series of concentration p:

$$S^{xx}(Q, \omega) = \sum_n^{\infty} p^n(1-p)^2 \bar{S}^{xx}_n(Q, \omega). \tag{3.2}$$

We calculate $\bar{S}^{xx}_n(Q, \omega)$ for $n \leq N$ and the contribution from the chains longer than N spins is estimated by extrapolation ($N = 16$ for $T = 0$ K and $N = 12$ for $T \neq 0$ K). Since the outline of $\bar{S}^{xx}_n(Q, \omega)$ converges with an increase of n, the contribution from the chains longer than N spins may be given as $\bar{S}^{xx}_N(Q, \omega)$ multiplied by a weight function $f_N(p)$. Thus, (3.1) is approximated as follows.

$$S^{xx}(Q, \omega) = \sum_n^{N} p^n(1-p)^2 \bar{S}^{xx}_n(Q, \omega) + f_N(p)\bar{S}^{xx}_N(Q, \omega). \tag{3.3}$$

Since the N-dependence of each peak is different, we use a different $f_N(p)$ for different peaks. For $\omega \sim 0$, there is no N-dependence because the number of domain walls

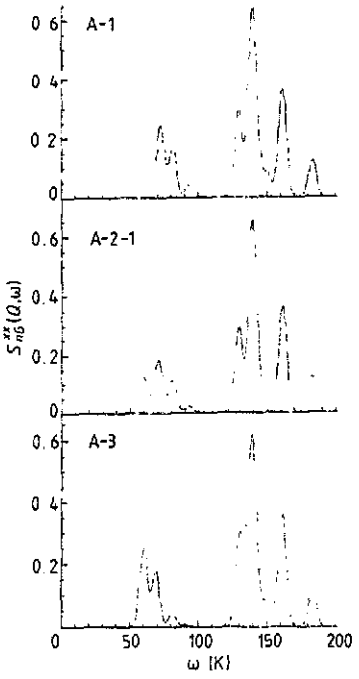

Figure 5. Effects of molecular fields on $S^{xx}_{nG}(Q, \omega)$ at $Q = \pi$ for $n = 9$. Data are convoluted by a Gaussian distribution with a half width at half maximum (HWHM) of 6.52 K.

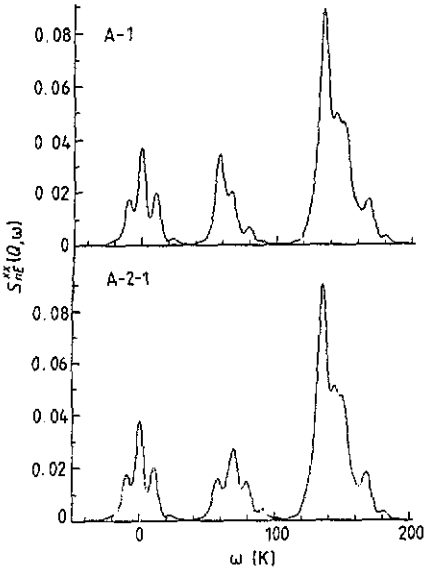

Figure 6. Effects of molecular fields on $S^{xx}_{nE}(q, \omega)$ at $Q = \pi$ for $n = 9$. Data are convoluted by a Gaussian distribution with a HWHM of 6.52 K.

conserves. For $\omega \sim J$, the peak grows linearly in proportion to the length of a chain, because this peak arises from the creation of one domain wall out of $N - 1$ possible sites. For $\omega \sim 2J$, we take into consideration the creation of two domain walls out of ${}_{N-1}C_2$ possible combinations. These three peaks are weakened by the factor of p every time one spin is added to a chain. Therefore, the function $f_N(p)$ may be given as

$$\text{(a)} \quad \omega \sim 0 \qquad f_N(p) = \sum_{k=N+1}^{\infty} p^k \tag{3.4a}$$

$$\text{(b)} \quad \omega \sim J \qquad f_N(p) = \sum_{k=N+1}^{\infty} \frac{k-1}{N-1} p^k \tag{3.4b}$$

$$\text{(c)} \quad \omega \sim 2J \qquad f_N(p) = \sum_{k=N+1}^{\infty} \frac{{}_{k-1}C_2}{{}_{N-1}C_2} p^k. \tag{3.4c}$$

Now we show the results for the dilute systems of $p = 0.70$, 0.83 and 0.90 at $T = 4.7$ and 30 K. Figure 7 presents the results for $T = 4.7$ K. The full curves represent the full values of (3.3) and the broken curves the first term of (3.3). The difference between the full curves and the broken curves becomes larger as p is increased. This is because the contribution of long chains increases in proportion to p. However, the results will still be reliable for $p = 0.90$ because the line shapes of the peaks are similar for chains longer than 12 spins. As p is increased, the relative intensity of the $\omega \sim J$ peak to the $\omega \sim 2J$

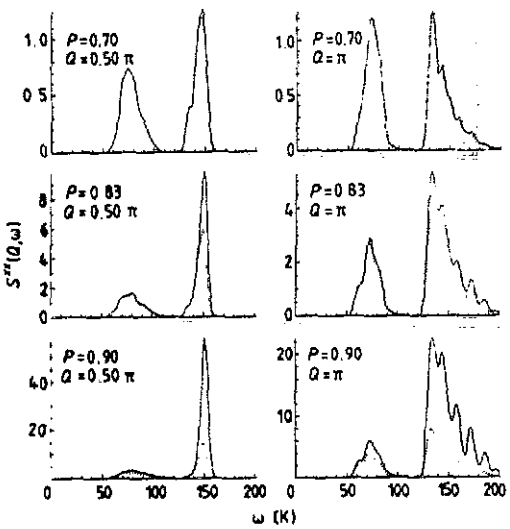

Figure 7. The results of dilute system for $T = 4.7$ K convoluted by Gaussian distribution with a HWHM of 6.52 K. Broken curves are the results before extrapolation.

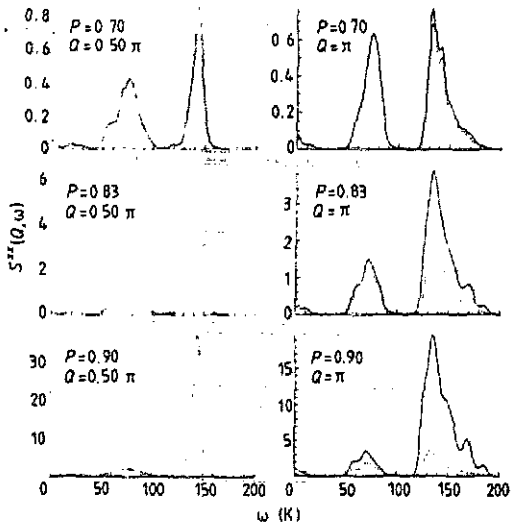

Figure 8. The results of dilute system for $T = 30$ K convoluted by a Gaussian distribution with a HWHM of 6.52 K. Broken curves are the results before extrapolation.

peak becomes smaller. The line shape of the $\omega \sim 2J$ peak changes as p is increased. The width of the peak becomes narrower at $Q = 0.5\pi$ and wider at $Q = \pi$. All these features are due to the enhancement of characters of long chains.

Figure 8 shows the results for $T = 30$ K. The $\omega \sim 0$ peak is seen, but its line shape depends little on p because the $\omega \sim 0$ mode does not depend strongly on the length of the chains. The $\omega \sim J$ and $2J$ peaks show similar features to those in the case of $T = 4.7$ K except that they are somewhat smooth.

To observe the $\omega \sim J$ peak in neutron scattering experiments, the peak should be sharp and comparable to the $\omega \sim 2J$ peak. These are satisfied when p is decreased, however, then the intensity becomes weak. The proper concentration to observe the $\omega \sim J$ peak will be $p = 0.7 \sim 0.8$.

4. Comparison with the experiment

In figure 9, our results are compared with experimental data for $p = 0.83$, at $T = 4.7$ K by Nagler *et al* (1984). The calculated $\omega \sim 2J$ peak fits the experimental data very well over the whole range of Q. The calculated $\omega \sim J$ peak also fits the experimental data at $Q = 0.5\pi$ but not so well at $Q = \pi$. The reason for this is not known at present. However, since the experimental data of the $\omega \sim J$ peak is not very clear, detailed experimental investigations are desired.

Values of the parameters used here are presented in table 1 together with those of previous works. The values are very similar to those used by Matsubara and Inawashiro (1991) and Matsubara *et al* (1991) in the case of $CsCoCl_3$.

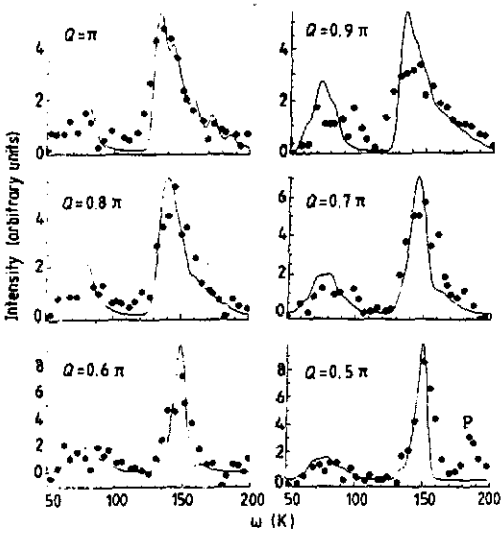

Figure 9. Comparison with the experimental data ($T = 4.7$ K, $p = 0.83$). Results are shown by full curves. Full circles are the experimental data by Nagler *et al* (1984). Values of parameters used in this comparison are given in table 1. 'P' indicates a phonon peak.

In the fittings, the role of J' is essentially important. The effect of J' is seen not only in the Q-dependence of the line shape of the $\omega \sim 2J$ peak but also in broadening of the $\omega \sim J$ peak.

5. Summary

We calculated the dynamical spin correlation function $S^{xx}(Q, \omega)$ of quasi-one-dimensional dilute antiferromagnet $CsCo_pMg_{1-p}Cl_3$ accumulating various finite chains. The results were in good agreement with the experimental observations by Nagler *et al* (1984).

Two peaks of $S^{xx}(Q, \omega)$ found in the experiment were identified as follows: the peak at $\omega \sim 2J$ ($\omega \sim 2J$ peak) is associated with soliton–pair excitations, and the peak at $\omega \sim J$ ($\omega \sim J$ peak), which is characteristic of the dilute system, is associated with single soliton excitations, where J is the intrachain nearest-neighbour interaction.

In this calculation, we took into account the intrachain next-nearest-neighbour interaction J'. From the fittings of the calculated $\omega \sim 2J$ peaks to the observed ones for different Q, we estimated $J'/J \sim 0.1$, which is compatible with that estimated by Matsubara and Inawashiro (1991) and Matsubara *et al* (1991). Hence, we believe this analysis confirms the existence of J'.

Attention was paid to the fact that the interchain interactions along the c-axis exist, because J' links two chains separated by a single Mg^{2+} ion. We took into account the interactions by molecular fields and found that they broaden the $\omega \sim J$ peak.

Our calculation suggested that, as the temperature is increased, another peak appears at $\omega \sim 0$.

Acknowledgment

The authors are indebted to Professor S E Nagler for suggesting to us that we analyse his experimental observations on $CsCo_pMg_{1-p}Cl_3$.

References

Breitling W, Lehmann W, Srinivasan T P and Weber R 1977a *J. Magn. Magn. Mater.* **6** 166
Breitling W, Lehmann W, Srinivasan T P, Weber R and Durr U 1977b *Solid State Commun.* **24** 267
Brietling W, Lehmann W, Srinivasan T P, Weber R, Leher N and Wagner V 1977c *J. Magn. Magn. Mater.* **6** 113
Hirakawa K and Yoshizawa H 1979 *J. Phys. Soc. Japan* **46** 455
Ishimura N and Shiba H 1980 *Prog. Theor. Phys.* **63** 743
Lehmann W P, Brietling W and Weber R 1981 *J. Phys. C: Solid State Phys.* **14** 4655
Matsubara F and Inawashiro S 1989 *J. Phys. Soc. Japan* **58** 4284
—— 1990 *Phys. Rev.* B **41** 2284
—— 1991 *Phys. Rev.* B **43** 796
Matsubara F, Inawashiro S and Ohhara H 1991 *J. Phys.: Condens. Matter* **3** 1815
Nagler S E, Buyers W J L, Armstrong R L and Briat B 1982 *Phys. Rev. Lett.* **49** 590
—— 1983a *Phys. Rev.* B **27** 1784
—— 1983b *Phys. Rev.* B **28** 3873
Nagler S E, Buyers W J L, Armstrong R L and Ritchie R A 1984 *J. Phys. C: Solid State Phys.* **17** 4819
Shiba H 1980 *Prog. Theor. Phys.* **64** 466
Villain J 1975 *Physica* **79B** 1
Yoshizawa H, Hirakawa K, Satija S K and Shirane G 1981 *Phys. Rev.* B **23** 2298